Endocranial Cast of Hexian *Homo erectus* from South China

Xiujie Wu,[1]* Lynne A. Schepartz,[2] Dean Falk,[3] and Wu Liu[1]

[1]*Institute of Vertebrate Paleontology and Paleoanthropology, Chinese Academy of Sciences, Beijing 100044, China*
[2]*Department of Anthropology, University of Cincinnati, Cincinnati, Ohio 45221-0380*
[3]*Department of Anthropology, Florida State University, Tallahassee, Florida 32306-7772*

KEY WORDS endocast; *Homo erectus*; Hexian; Zhoukoudian; brain evolution

ABSTRACT In this paper, we present data on the morphological features and linear measurements for the Hexian *Homo erectus* and other comparative endocasts, in order to highlight variation during human brain evolution. The endocast of Hexian was reconstructed in 1982, and an endocranial volume of 1,025 ml was estimated. The geological age is about 412 ka, or roughly contemporaneous with the Zhoukoudian (ZKD) specimens. There are some differences between Hexian and the modern Chinese male endocasts in our sample, including low position of the greatest breadth, low maximum height, a well-marked and prominent frontal keel, the flat surface of the frontal lobes, prominent sagittal keel along the center frontal and parietal lobes, depressed Sylvian areas and parietal lobes superiorly, strong posterior projection of the occipital lobes, anterior position of the cerebellar lobes relative to the occipital lobes, and the relative simplicity of the meningeal vessels. Compared with the ZKD, Indonesian, and African *Homo erectus* specimens, Hexian has more morphological features in common with ZKD. Principal component analyses indicate that Hexian is closest to the ZKD *Homo erectus* compared with the modern Chinese and other *Homo erectus*, but its great breadth distinguishes it. Metric analyses show that the brain height, frontal breadth, cerebral height, frontal height, and parietal chord from *Homo erectus* to modern humans increased, while the length, breadth, frontal chord, and occipital breadth did not change substantially. Am J Phys Anthropol 130:445–454, 2006.

The Hexian cranium was found in 1980 in Longtandong (118°20′ East, 31°35′ North), Hexian county, Anhui province, in southern China (Fig. 1) (Huang et al., 1981). The cranium was deformed and broken into several fragments (Wu and Poirier, 1995). After reconstruction, however, the skull is rather complete, although it lacks most of the basicranium (Fig. 2). An endocast was reconstructed from the skull in 1982, and was determined to have an estimated volume of 1,025 ml. The endocast reproduces almost complete frontal and temporal lobes, and complete parietal and occipital lobes. The missing elements include the base of the frontal lobe, the base of the left temporal lobe, the anterior basal portion of the right temporal lobe, and the area of the foramen magnum (Fig. 3).

The age of the Hexian hominid was estimated from faunal correlations and several geochemical studies. An age of about 200 ka was initially assigned to the site (Huang et al., 1982). The thermoluminesence (TL) date on quartz is 195 ± 16 ka (Li and Mei, 1983). A U-series dating of faunal bone yielded ages in the range of 150–270 ka (Chen et al., 1987), while electron spin resonance (ESR) studies yielded results of about 300 ka for mammalian teeth (Huang et al., 1995). Most recently, combined ESR and U-series analyses obtained an age estimate of 412 ± 25 ka (representing an average of six analyses on two teeth) (Grün et al., 1998). These age estimates imply that the Hexian *Homo erectus* was contemporaneous with the Zhoukoudian (ZKD) X, XI, and XII specimens (Huang et al., 1993).

The taxonomic affinity of Hexian and ZKD has been subject to question. Several researchers demonstrated that the Hexian cranium possesses many characteristics that are typical of *Homo erectus*, including a low position for the maximum vault breadth, thick cranial bones, strong development of the torus supraorbitalis and torus angularis, and well-developed supramastoid crests and torus occipitalis (Wu and Dong, 1982). Comparisons of this specimen to other *Homo erectus* from China and Java suggested to some workers that Hexian is most similar to ZKD *Homo erectus*. These researchers interpreted the morphological differences between Hexian and ZKD as indications of local variations rather than differences at a subspecies level (Huang et al., 1981; Wu and Dong, 1982; Wu and Poirier, 1995). Kidder and Durband (2004), on the other hand, concluded that the Hexian calvarium resembles African and Indonesian *Homo erectus* specimens, and differs significantly from the craniometrical pattern of the ZKD fossils, which is consistent with the argument that the Chinese sample from ZKD does not fully represent the range of variation seen within Asian *H. erectus* (Antón, 2002a,b, 2003).

The purpose of this paper is to describe and interpret the morphology of the Hexian *Homo erectus* endocast,

Grant sponsor: Taft Memorial Fund, University of Cincinnati; Grant sponsor: National Science Fund for Fostering Talents in Basic Research, Special Research Disciplinary Unit (Paleontology and Paleoanthropology), China.

*Correspondence to: Xiujie Wu, Institute of Vertebrate Paleontology and Paleoanthropology, Chinese Academy of Sciences, PO Box 643, Beijing 100044, China. E-mail: wuxiujie@126.com

Received 5 January 2005; accepted 8 September 2005.

DOI 10.1002/ajpa.20378
Published online 19 January 2006 in Wiley InterScience (www.interscience.wiley.com).

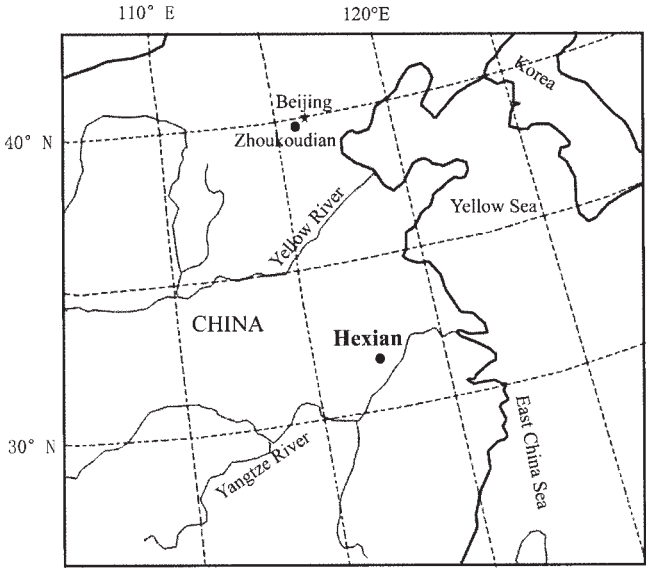

Fig. 1. Map showing location of Hexian, China.

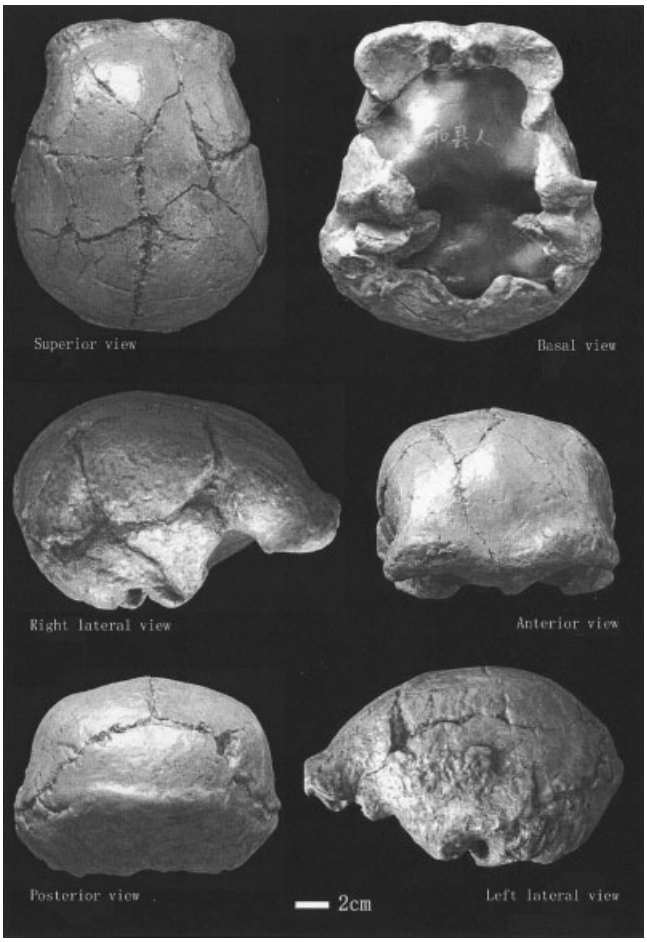

Fig. 2. Skull of Hexian *Homo erectus*.

and to compare its morphology with other *Homo erectus* (ZKD, KNM-WT 15000, and Sm 3), in order to develop a broader picture of variation and evolution in this taxon generally. We regard this as an important step in the growing record of early hominid brain evolution.

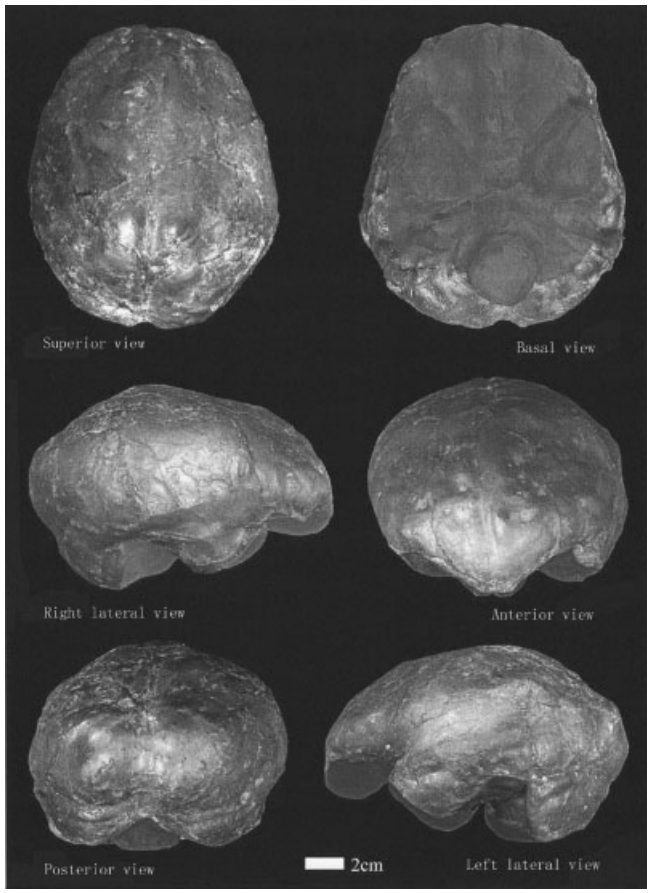

Fig. 3. Endocast of Hexian *Homo erectus*.

MATERIALS

Endocasts of eight *Homo erectus* and 31 modern Chinese were studied (Table 1). Hexian, ZKD II (Skull II, Locus D), ZKD III (Skull III, Locus E), ZKD X (Skull X, Locus L I), ZKD XI (Skull XI, Locus L II), and ZKD XII (Skull XII, Locus L III) are from the collections of the Institute of Vertebrate Paleontology and Paleoanthropology, Chinese Academy of Sciences. Because Hexian is male, we chose 31 male, adult modern Chinese skulls for silicone rubber endocast reconstruction. These modern Chinese skulls were anatomical specimens from Hebei province. These skulls had been cut into two parts from the middle of the cranium on the coronal plane. Silicone rubber was applied to the interior of both parts of the cranium with a brush in a swirling motion. In total, three layers of silicone rubber and one layer of gauze were applied, and then the two halves were rejoined. After the silicone rubber set, the endocast was removed from the interior of the cranium. The endocast was then filled with cotton batting through the foramen magnum to maintain its shape. Each endocast was made using this technique. Comparative measurements between the endocast and endocranium show shrinkage of less than 1 mm.

The observations and metric data for the endocasts of Sm 3 (Broadfield et al., 2001; Delson et al., 2001) and

TABLE 1. Endocasts of Homo erectus *used in the study*

Endocast	Date (ka)	Sex	Age	Cranial capacity (cc)
Hexian	412[1]	M	Adult	1,025[5]
ZKD III (Skull E I)	423[2]	M	Juvenile	915[6]
ZKD II (Skull D I)	585[2]	F	Adult	1,020[6]
ZKD X (Skull L I)	423[2]	M	Adult	1,225[6]
ZKD XI (Skull L II)	423[2]	F	Adult	1,015[6]
ZKD XII (Skull L III)	423[2]	M	Adult	1,030[6]
Sm 3	>100[3]	F	Adult	917[7]
KNM-WT 15000	1,530[4]	M	Juvenile	880[4]
Modern Chinese (n = 31)		M	Adult	1,140–1,540

[1] Grün et al. (1998).
[2] Huang et al. (1993).
[3] Delson et al. (2001).
[4] Begun and Walker (1993).
[5] Wu and Dong (1982).
[6] Weidenreich (1943).
[7] Broadfield et al. (2001).

KNM-WT 15000 (Begun and Walker, 1993) were based on published papers.

MORPHOLOGICAL FEATURES

Gross morphology

The Hexian endocast is short and wide, with an ovoid form in superior view. The widest point is situated at the lateral border of the temporal lobes. In terms of overall height, Hexian is proportionally low when compared to its maximum length and width dimensions.

Frontal lobe. The form of the frontal lobes when observed in frontal view (Fig. 4) is triangular, and the orbital margin is full and culminates in a well-marked and prominent frontal keel, similar to the form seen on the endocasts of ZKD. The shape of the frontal lobe is relatively flat compared to modern humans. The impression of the metopic suture is visible between the frontal pole and bregma, and numerous gyri and sulci are observable (Fig. 5). The area of the inferior frontal gyrus is slightly larger and more prominent on the left side than on the right (Figs. 6, 7).

Sagittal keel. Between bregma and the vertex on the parietals, Hexian displays a prominent area that is evident on both the endocast and the cranium. On the cranium, this appears as a clear sagittal keel that involves the parietals and the frontal. Correspondingly, the endocast has a sagittal keel (Figs. 4, 5) along the center frontal lobe and parietal lobes.

Parietal lobe. The parietal lobes are depressed superiorly and bossed inferiorly and laterally on both sides relative to the rounded form seen in modern humans. The vertex of the endocast is very prominent and located in the middle of the centro-parietal lobe. From the vertex (Figs. 4, 5), the brain contour slopes downward in all directions. Posteriorly it slopes sharply backward to the occipital pole, while anteriorly the surface slopes forward to the frontal pole (Figs. 6, 7). Laterally, the endocast surface slopes to the parietal eminence, then toward the temporal lobe (Fig. 8).

Temporal pole. The temporal region is wide. The course of the Sylvian fissure is clearly reproduced on the left side, and the endocast is beveled on the lower border of the frontal lobe and the upper border of the temporal pole (Fig. 7). The fissure does not appear on the right side (Fig. 6).

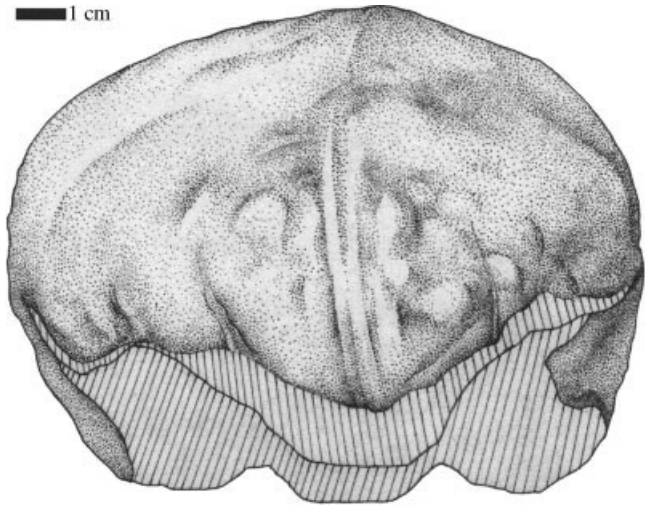

Fig. 4. Diagrammatic drawing of anterior view of Hexian endocast.

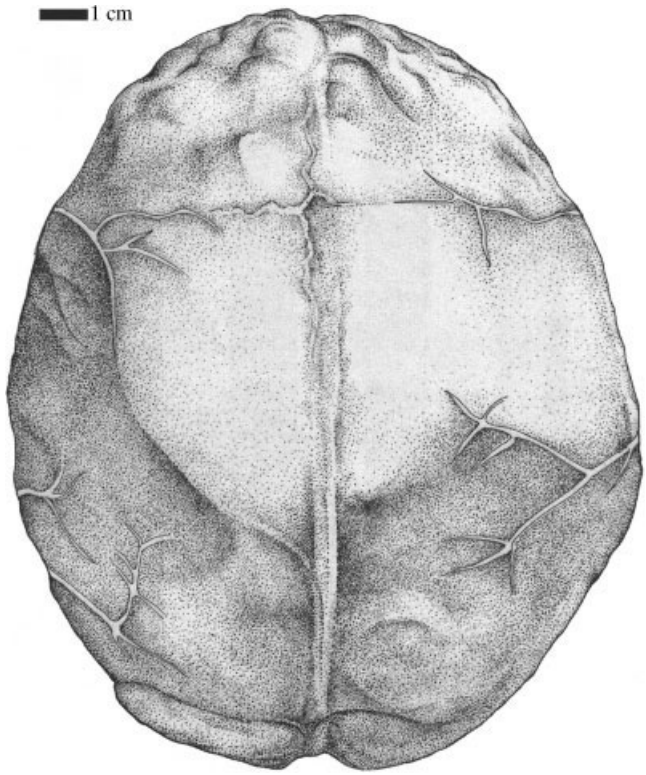

Fig. 5. Diagrammatic drawing of superior view of Hexian endocast.

Occipital lobe. On the other hand, when the endocast is viewed posteriorly (Fig. 8), the lambdoidal suture appears to approximate the rostral limit of the occipital lobe. The superior portion of the occipital lobe forms a semicircular shape, and the occipital poles are especially prominent and rounded.

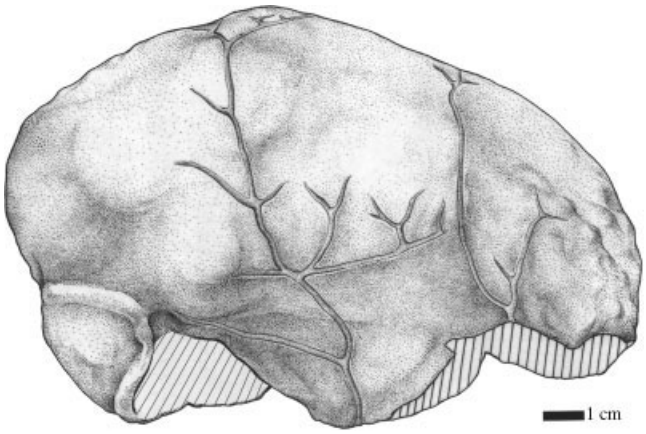

Fig. 6. Diagrammatic drawing of right lateral view of Hexian endocast.

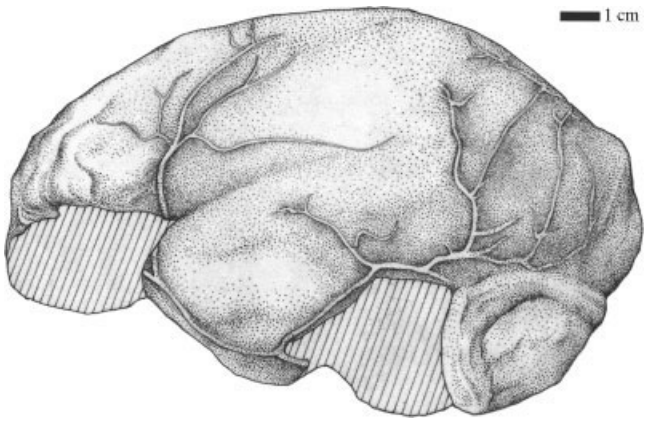

Fig. 7. Diagrammatic drawing of left lateral view of Hexian endocast.

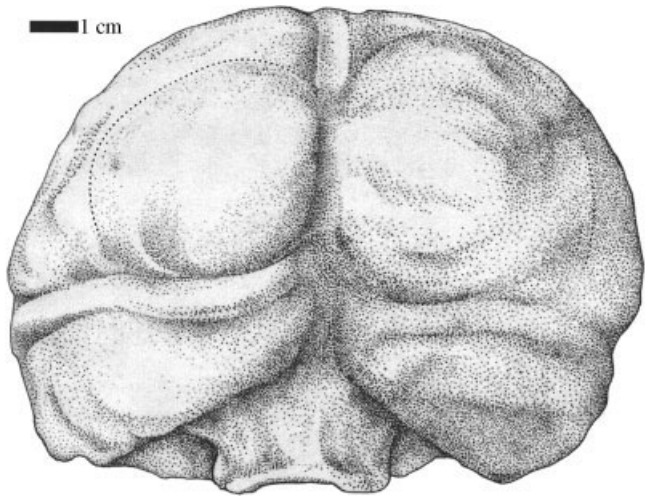

Fig. 8. Diagrammatic drawing of posterior view of Hexian endocast.

Meningeal vessels. Although the meningeal vessels appear clearly on both sides of the Hexian endocast, as described for the other *Homo erectus* endocasts analyzed by Weidenreich (1938), their identification is problematic (Falk, 1993). The confusion arises because Weidenreich (1938) applied the antiquated scheme of Adachi (1928) for classifying human meningeal vessels to *Homo erectus* endocasts, rather than interpreting them in light of comparative data from apes and humans. In so doing, the meningeal supply to the middle braincase that stemmed from the orbit rather than the floor of the middle cranial fossa was not recognized, which sometimes caused the anterior (and other) branches of the middle meningeal vessels to be misidentified (details in Falk, 1993). Thus, the most rostral meningeal arterial supply represented in both hemispheres of the Hexian endocast may well stem from a branch of the internal carotid artery that emerges from the region near the superior orbital fissure, rather than from the anterior branch of the middle meningeal artery, which traces to the foramen spinosum and ultimately derives its blood from the external carotid artery (Falk, 1993). If so, upon entering the middle cranial fossa, the middle meningeal vessels of the left hemisphere of Hexian divide into a short anterior branch that courses toward the temporal pole, and a much longer posterior branch that courses caudally and becomes elaborated in the region of the occipital parietal cortex (Fig. 7). This pattern comes closest to pattern A3 or A4 seen in apes and *Homo erectus* endocasts from the left sides of Skull H (ZKD V, Locus H) and Skull II (ZKD XI, Locus II), and both sides of Skull E (ZKD III, Locus E) (Falk, 1993). Unlike the left hemisphere, however, upon entering the skull, the middle meningeal vessels on the right side branch into a simple posterior branch that does not become elaborated caudally, and an anterior branch that courses toward the vertex after giving off a rostral coursing branch at about the level of the superior temporal gyrus (Fig. 6). Other interpretations are possible, of course. For example, Wu and Dong (1982) described the most rostral branches on the Hexian endocast as the anterior branches of the middle meningeal vessels, rather than as meningeal contributions stemming from near the orbital fissure, as proposed by Falk (1993). They therefore concluded that the posterior branch of the middle meningeal vessels was larger than the anterior ones. In any event, what stands out about the meningeal vascular pattern of Hexian is its simplicity, even compared to other *Homo erectus* endocasts (Weidenreich, 1938). This is interesting in light of the reasonable suggestion by Weidenreich (1938, p. 12) that the blood supply to the parietal bone extending from vertex to lambda became more elaborated during the subsequent course of hominid cranial expansion.

Venous sinuses. The superior sagittal sinus is visible, beginning as a narrow ridge between the rostral cerebral poles that becomes more marked at the vertex of the centro-parietal pole. At lambda, the vessel deviates somewhat to the left. At the confluence, the superior sagittal sinus bifurcates. One branch is continuous with the left transverse sinus, sweeping forward and downward to the left sigmoid sinus and then into the left jugular region. Another branch is continuous with the right transverse sinus. It flows forward and downward to the right sigmoid sinus, and then into the right jugular region. The transverse sinus is wider on the left side (Fig. 8).

Petalial patterns. The method for determining frontal and occipital petalial patterns derives from LeMay et al. (1982), who scored which hemisphere protruded

TABLE 2. Morphological features of Hexian, other Homo erectus, *and modern Chinese endocasts*

	Hexian	ZKD	KNM-WT 15000	Sm 3	Modern humans
1. Widest point	Low	Low	Low	High	Most in middle
2. Frontal lobe	Flat	Flat	Flat	Round	Round
3. Frontal keel	Present	Present	Absent	Absent	Absent
4. Orbital "cap"	Left > right	Left > right	Left > right	Left > right	Left > right
5. Sagittal keel	Present	Present	Absent	Absent	Some present
6. Sylvian area	Left depression and right flat	Distinct depressions	No distinct depressions	No distinct depressions	No depression
7. Parietal lobe	Depressed and sloping	Depressed and sloping	Round	Round	Round
8. Temporal lobe	Wide and flat	Narrow, slender, and flared	Wide and less flared	Wide and less flared	Wide and flared
9. Occipital lobe	Flattened, projection	Flattened, projection	Round, no projection	Round, no projection	Round, projecting
10. Cerebellar lobe	Anterior to occipital lobe	Anterior to occipital lobe	Projects posterior	Anterior to occipital lobe	Projects posterior
11. Meningeal vessels	Orbital contribution to middle cranial fosse	Orbital contribution to middle cranial fosse	Extent of orbital contribution unknown	Extent of orbital contribution unknown	Obtains its blood from external carotid
12. Superior sagittal sinus at confluence	Two branches	Deviates to right	Deviates to right	Deviates to left	Three kinds of type
13. Petalial pattern	R-frontal and R-occipital	R-frontal and R-occipital; L-frontal and R-occipital; L-frontal and L-occipital	R-frontal and L-occipital	R-frontal and L-occipital	R-frontal and L-occipital (ca 90%)

further rostrally (for the frontal petalia) and caudally (occipital petalia), in addition to which hemispheres were widest. Since that pioneering work, it has become clear that protrusion petalias are extremely difficult to score because they can change with the slightest rostral or caudal rotation of an endocast. Thus, petalias are more likely to be reliably scored by comparing widths rather than rostral/caudal projections (Zilles et al., 1996). A photograph was taken of the superior view of the endocast, oriented such that a line through the rostral and caudal poles of each hemisphere was aligned horizontally. Measurements were made in the picture at a scale of 1 to 1. For the frontal patalia, the lateral width from the midsagittal plane in both directions was measured from the point along the midsagittal axis located 20% of the distance from the perpendicular plane, marking the most anterior point of the frontal lobes, to the perpendicular plane, marking the most posterior point of the occipital lobes. For the occipital petalia, lateral width from the midsagittal plane in both directions was measured from the point along the midsagittal axis located 10% of the length forward along the same midsagittal axis from the perpendicular plane, marking the most posterior point of the occipital lobes. Using this method, Hexian manifests right frontal and right occipital petalia width patterns.

Comparison with other *Homo erectus* endocasts

Table 2 provides comparisons of 13 morphological features of Hexian, other *Homo erectus*, and modern Chinese male endocasts. In general, the widest point or greatest breadth of most modern Chinese in our sample is situated at the middle position. In *Homo erectus*, the widest point is usually in a low position. The surfaces of the frontal lobe of Hexian, the ZKD endocasts, and KNM-WT 15000 are flat, whereas the frontal lobes of Sm 3 and modern Chinese are filled out and rounded. The frontal keel is prominent on Hexian and ZKD, but is not seen on KNM-WT 15000 and Sm 3. The orbital margin is round, and no prominent frontal keel is seen in the modern Chinese. The area of the inferior frontal gyrus is slightly larger and more prominent on the left side in all *Homo erectus* and modern Chinese specimens compared here. Both Hexian and the ZKD endocasts have sagittal keels and depressed Sylvian areas (seen only on the left for Hexian), in contrast to the flat regions that characterize KNM-WT 15000 and Sm 3. Some of the modern Chinese in our sample have a weak sagittal keel, but no depressed Sylvian areas. Superiorly, the parietal lobes of both Hexian and ZKD are depressed, and slope downward in all directions from the centro-vertex, while in the modern Chinese, the parietal lobes are altogether rounded and full. The temporal lobes of Hexian are wide, similar to those of KNM-WT 15000, Sm 3, and the modern Chinese, and different from the ZKD specimens that are narrow and slender. The occipital lobes of both Hexian and ZKD are dorso-ventrally flattened and have a strong posterior projection. In contrast, the lobes of KNM-WT 15000, Sm 3, and the modern Chinese are round and lack strong posterior projections. The cerebellar lobes are anterior to the occipital lobe for Hexian, ZKD, and Sm 3. They project posteriorly almost as much as the occipital lobes for KNM-WT 15000, Sm 3, and the modern Chinese. The meningeal vessels are similar on both Hexian and the ZKD endocasts, and differ from the modern Chinese. The venous-sinuses pattern varies among specimens. In modern humans, there are three main patterns at the confluence of the superior sagittal sinus flow (Li et al., 2000): 1) the superior sagittal sinus is divided into two branches, and the size of the left transverse is similar to the right one (42.7%); 2) the superior sagittal sinus deviates to the right (52%), and the transverse sinus is wider on the right side than on the left; and 3) the superior sagittal sinus deviates to the left (5.3%), and the transverse sinus is wider on the left side than on the right. For *Homo erectus*, the venous-sinuses pattern variation is similar to that in modern humans, and the specimens studied here exhibit all three patterns. The petalial patterns in most modern humans are right (R)-frontal petalial and left (L)-occipital patalial (LeMay, 1976, 1982; Galaburda et al, 1978; Holloway et al, 1982; Zilles et al., 1996). This pattern is also seen in KNM-WT 15000 and Sm 3. Hexian and ZKD III manifest R-frontal and R-occipital petalial width patterns, while the other endocasts show L-frontal and R-occipital (ZKD X) or L-frontal and L-occipital (ZKD XI and XII) patterns.

TABLE 3. List of landmarks with their definitions

Landmark	Definition
FP	Most anterior protuberance of frontal lobe
OP	Most posterior protuberance of occipital lobe
IB	Intersection of coronal and sagittal sutures on inside of braincase
IL	Intersection of lambdoidal and sagittal sutures on inside of braincase
IEU	Greatest lateral protrusion point of endocast
FB	Greatest lateral protrusion point of frontal lobe
OB	Greatest lateral point of occipital lobe
PH	Highest point of parietal lobe
FI	Most ventral point of frontal lobe
TI	Most ventral point of temporal lobe
CI	Most ventral point of cerebellar hemisphere

METRICAL COMPARISONS

Methods

Linear measures and indices were taken to provide quantification of the overall shape of the endocast. We chose 11 landmarks (Table 3) and nine standardized measurements (Fig. 9), following Begun and Walker (1993). Because they did not describe their method in detail, we measured the endocast according to our methods. In order to standardize the measuring procedure, each endocast was placed on a flat surface, with the horizontal plane along the axis of the frontal and occipital poles (right side) parallel to the flat surface. The endocast remained with the axis of the frontal and occipital poles parallel to the flat surface, whether rotated for a superior or lateral view. FB usually refers to the most posterior position of the frontal lobe. Because the central sulcus is not visible on the endocasts in our sample, FB was marked as the greatest protrusion of the frontal lobe (see Table 3 for expansions of abbreviations). OB was determined by the greatest lateral protrusion of the occipital lobe. For length (FP-OP), we used the greater of the two hemisphere lengths. For breadth (IEU-IEU), we measured the maximum width perpendicular to the sagittal plane. For height (PH-CI), cerebral height (PH-TI), frontal height (IB-FI), and the frontal chord (IB-FP), we used the right side. For frontal breadth (FB-FB) and occipital breadth (OB-OB), we measured the maximum width of the frontal lobe and the occipital lobe perpendicular to the sagittal plane. Measurements were taken with sliding and spreading calipers and recorded to the nearest 0.1 mm. Each endocast was measured three times, and the average was used as the final measurement. The measurement error mean is below 2.5%. Statistical analyses were performed using SPSS (version 11.0). Independent-samples nonparametric tests (Kruskal-Wallis test) were used to determine whether fossils were different from the modern Chinese in our sample. Standard deviation (SD) was used for dispersion around the mean. We constructed bivariate plots, and performed principal component analyses (PCAs) to look at interactions among variables. In bivariate plot comparisons, length, breadth, and height were used, and linear regression analysis with 95% confidence intervals showed the range of the modern Chinese. For PCAs, two analyses were run, one with all nine variables, and the other including only the five measurements for which all fossils were significantly different from the modern Chinese in our sample.

Statistical results

Metric data on Hexian, ZKD, Sm 3, KNM-WT 15000, and the modern Chinese in our sample are included in Table 4. The average length is 161.7 (measurements in mm) (SD = 7.3; range, 151.1–174.2) for the fossils, and 168.3 (SD = 4.3; range, 159.8–177.0) for the modern Chinese. The breadth is 123.1 for the fossils (SD = 7.6; range, 113.6–134.8), and 127.5 (SD = 5.6; range, 117.0–137.3) for the modern Chinese. The frontal chord is 76.2 (SD = 5.7; range, 69.1–85.3) for the fossils, and 78.8 (SD = 5.3; range, 69.2–89.0) for the modern Chinese. The occipital breadth is 94.5 (SD = 4.7; range, 87.3–103.0) for the fossils, and 98.6 (SD = 3.6; range, 91.5–107.5) for the modern Chinese. There were no statistically significant differences between *Homo erectus* and the modern Chinese in our sample. Also, Hexian was grouped with *Homo erectus* for these calculations.

The differences were statistically significant for height, frontal breadth, cerebral height, frontal height, and parietal chord between *Homo erectus* and the modern Chinese in our sample. The height is 105.1 for the fossils (SD = 5.2; range, 99.7–114.2), and 127.2 (SD = 3.3; range, 119.8–135.2) for the modern Chinese. The frontal breadth is 97.4 (SD = 6.1; range, 86.0–106.7) for the fossils, and 112.0 (SD = 5.1; range, 102.9–122.3) for the modern Chinese. The cerebral height is 105.7 (SD = 5.3; range, 98.9–116.2) for the fossils, and 121.8 (SD = 4.9; range, 110.9–133.8) for the modern Chinese. The frontal height is 77.0 (SD = 6.3; range, 66.0–88.2) for the fossils, and 91.5 (SD = 3.6; range, 86.1–99.9) for the modern Chinese. The parietal chord is 90.0 (SD = 4.5; range, 82.9–95.9) for the fossils, and 105.5 (SD = 3.7; range, 97.9–114.1) for the modern Chinese. These five calculations separate *Homo erectus* from the modern Chinese in our sample.

The breadth-length index (ratio of breadth to length; Table 4) is traditionally used to group endocasts into broadly descriptive brachycephalic (0.80–0.90), mesocephalic (0.76–0.79), and dolichocephalic (0.71–0.75) categories (Weidenreich, 1939). Most modern Chinese in our sample fall within the mesocephalic and dolichocephalic groups, although some fall within the brachycephalic group. The brain shape of Hexian, with an index of 0.85, falls within the brachycephalic group, and is distinct from the other *Homo erectus* specimens. ZKD III (0.77), ZKD XI (0.77), and ZKD XII (0.76) are mesocephalic; ZKD II (0.72), ZKDX (0.74), Sm 3 (0.75), and KNM-WT 15000 (0.73) fall within the dolichocephalic range. These distinctions are only useful for describing endocasts, and may well have no taxonomic or behavioral significance. The main differences between *Homo erectus* and the modern Chinese are the height-breadth and height-length indices, which are lower for all *Homo erectus* specimens. All *Homo erectus* specimens are very similar in terms of the height-length index. Conversely, the height-breadth index of Hexian is 0.75, which is much lower than the other specimens.

According to the bivariate plot of length and height (Fig.10), all *Homo erectus* are beyond the range of linear regression, with a 95% individual prediction interval for the modern Chinese in our sample, and are much lower than the modern Chinese in height. Hexian clusters with KNM-WT 1500 and ZKD III. In the plot of breadth and height (Fig. 11), Hexian is considerably wider than the other *Homo erectus*, but is still in the range of the modern Chinese in our sample.

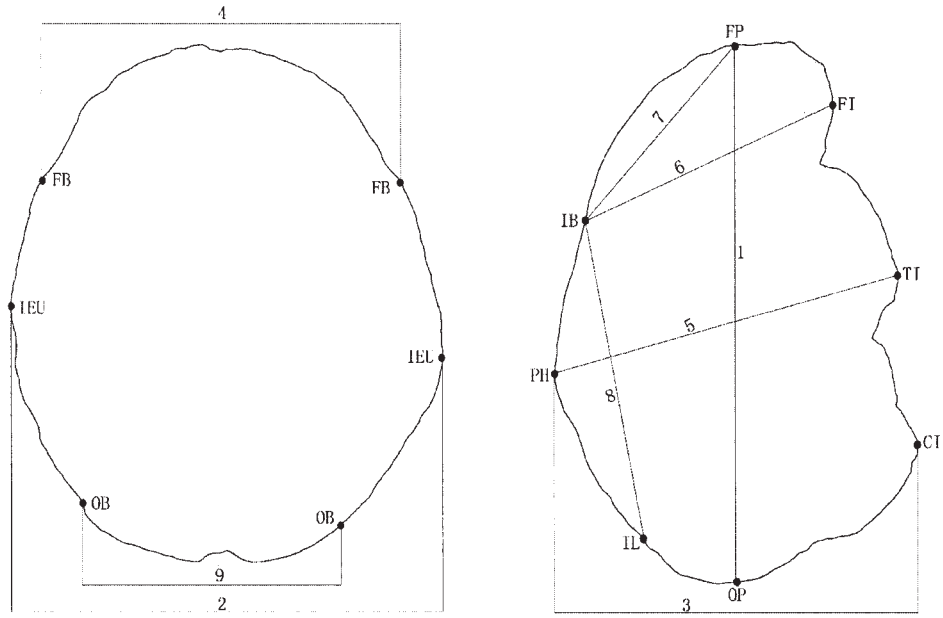

Fig. 9. Superior and right lateral views of Hexian endocast, showing landmarks and measurements used. 1, length; 2, breadth; 3, height; 4, frontal breadth; 5, cerebral height; 6, frontal height; 7, frontal chord; 8, parietal chord; 9, occipital breadth. For abbreviations, see Table 3.

TABLE 4. Endocasts measurements (mm), indices and nonparametric-tests of Homo erectus *and the modern Chinese*[1]

Measurement or index	Hexian	ZKD II	ZKD III	ZKD X	ZKD XI	ZKD XII	Sm 3[2]	KNM-WT 15000[3]	He[4] (mean)	He[4] (SD)	MC[5] (mean)	MC[5] (SD)	MC[5] (range)	Asymp. sig[6]
1. Length	159.4	161.1	156.1	174.2	166.1	167.6	151.1	158.0	161.7	7.3	168.3	4.3	159.8–177.0	0.067
2. Breadth	134.8	116.2	120.4	128.7	127.2	127.8	113.6	116.0	123.1	7.6	127.5	5.6	117.0–137.3	0.189
3. Height	100.7	106.4	99.7	114.8	103.7	108.5	107.2[7]	100.0	105.1	5.2	127.2	3.3	119.8–135.2	0.015*
4. Frontal breadth	99.8	94.2	91.9	106.7	97.1	97.8	103.5[7]	86.0	97.4	6.1	112.0	5.1	102.9–122.3	0.025*
5. Cerebral height	102.0	107.2	98.9	116.2	105.4	107.3	101.3	107.0	105.7	5.3	121.8	4.9	110.9–133.8	0.019*
6. Frontal height	75.9	78.2	73.1	88.2	79.0	79.9	75.0[7]	66.0	77.0	6.3	91.5	3.6	86.1–99.9	0.024*
7. Frontal chord	69.1	75.9	78.2	85.3	70.2	82.6	73.0[7]	73.0	76.2	5.7	78.8	5.3	69.2–89.0	0.272
8. Parietal chord	92.2	94.5	86.9	95.9	87.2	87.5	82.9	93.0	90.0	4.5	105.5	3.7	97.9–114.1	0.015*
9. Occipital breadth	96.6	89.9	87.3	95.5	93.3	95.0	95.6	103.0	94.5	4.7	98.6	3.6	91.5–107.5	0.158
Breadth/length	0.85	0.72	0.77	0.74	0.77	0.76	0.75	0.73			0.76		0.70–0.82	0.621
Height/breadth	0.75	0.92	0.83	0.89	0.82	0.85	0.94	0.86			1.00		0.93–1.09	0.015*
Height/length	0.63	0.66	0.64	0.66	0.62	0.65	0.71	0.63			0.76		0.72–0.81	0.014*

[1] Descriptions for measurements 1–9 may be found in legend for Figure 9.
[2] Broadfield et al. (2001).
[3] Begun and Walker (1993).
[4] He, *Homo erectus*.
[5] MC, modern Chinese.
[6] Comparision is between fossils vs. modern Chinese.
[7] Estimate.
*$P < 0.05$.

The PCAs provide further information on the overall shape of the *Homo erectus* endocasts. In the nine-variable analysis, the first two components account for 71.4% of the total variance (Table 5). The first component (60.5%) has positive loadings on all variables, and is mainly related to height and frontal height. The second component (10.9%) is mainly related to the frontal chord. In Figure 12, Hexian is close to the other *Homo erectus* specimens (with the exception of ZKD X), and distant from the modern Chinese for PC1. For PC2, Hexian is closest to Sm 3, KNM-WT 15000, ZKD II, ZKD III, ZKD XI, and the majority of the modern Chinese. Overall, Hexian clusters with Sm 3, ZKD III, ZKD XI, ZKD II, and KNM-WT 15000.

In the five-variable PCA (Table 5), we chose the variables which were statistically significant (height, frontal breadth, cerebral height, frontal height, and parietal chord). The first and second principal components represent 83.9% and 6.8% of the total variance. The first component is related to height and frontal height, and the second component is related to frontal breadth and frontal height. In Figure 13, Hexian clusters with ZKD.

DISCUSSION

The frontal lobes are one of the most studied areas on fossil endocasts because of their presumed role in higher cognitive functions and language. The area of the inferior frontal gyrus (the orbital "cap") is slightly larger and more prominent on the left than on the right side on all specimens compared in this study. Many researchers (Black, 1930, 1931, 1932, 1933; Weidenreich, 1939; Aboitiz and Garcia, 1997; Broadfield et al., 2001) noted that the left orbital "cap" (which contains a homologue of part of Broca's area, i.e., Brodmann's area 44 in apes, but

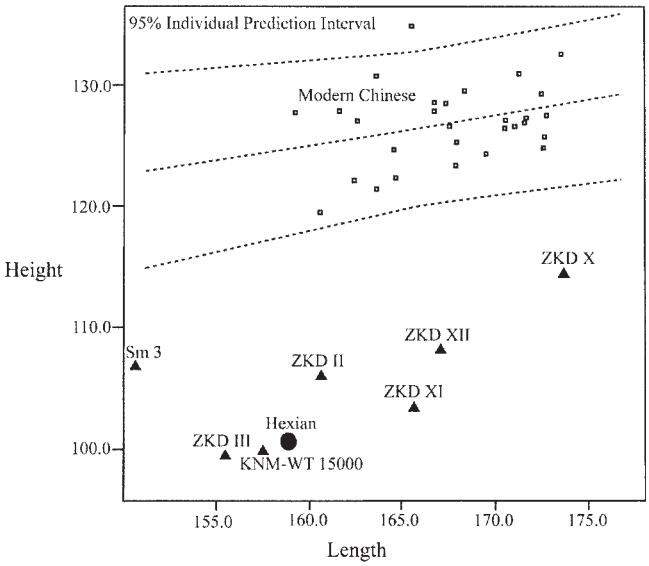

Fig. 10. Bivariate morphometric comparison of length and height among Hexian, other *Homo erectus*, and modern Chinese.

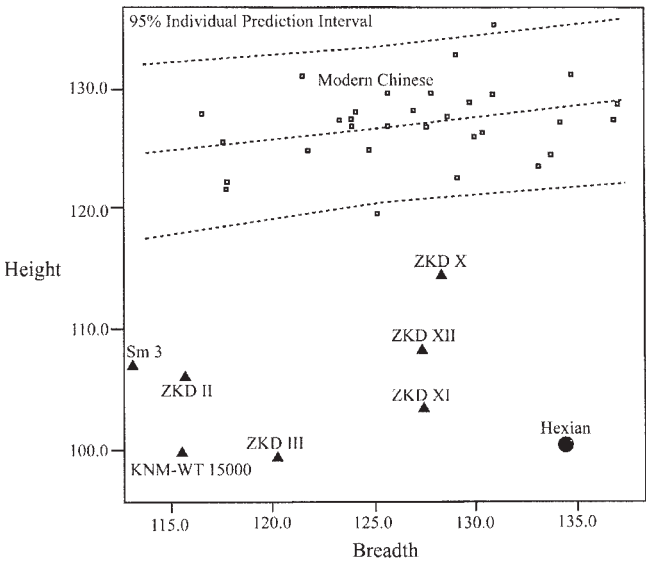

Fig. 11. Bivariate morphometric comparison of breadth and height among Hexian, other *Homo erectus*, and modern Chinese.

contains areas 45 and 47 in humans; details in Falk, 2006) is bigger than the right in fossil human endocasts, and that this asymmetry suggests that *Homo erectus* possibly had the ability to speak. However, some authors (Amunts et al., 1999) also suggested that areas 45 and 44 (true Broca's area in humans) cannot be reliably and precisely located on the basis of contours, and that it is therefore difficult to ascertain speech or language capability from endocasts. While the issue of identifying specific areas remains open to debate, this frontal asymmetry is certainly a noteworthy characteristic of *Homo erectus* that deserves further investigation. Linking information about the frontal lobe morphology of endocasts to cranial frontal morphology may help clarify the differ-

TABLE 5. Principal components analysis loadings: nine-variable and five-variable analyses of Hexian, other Homo erectus, *and modern Chinese endocasts*

	Nine-variable		Five-variable	
Variable	PC 1	PC 2	PC 1	PC 2
Length	0.144	0.419		
Breadth	0.110	0.216		
Height	0.168	−0.278	0.229	−0.279
Frontal breadth	0.156	−0.185	0.206	1.376
Cerebral height	0.163	−0.244	0.221	−0.482
Frontal height	0.166	−0.132	0.222	0.280
Frontal chord	0.087	0.744		
Parietal chord	0.162	−0.163	0.214	−0.821
Occipital breadth	0.102	0.148		
Percent of variance	60.5%	10.9%	83.9%	6.8%

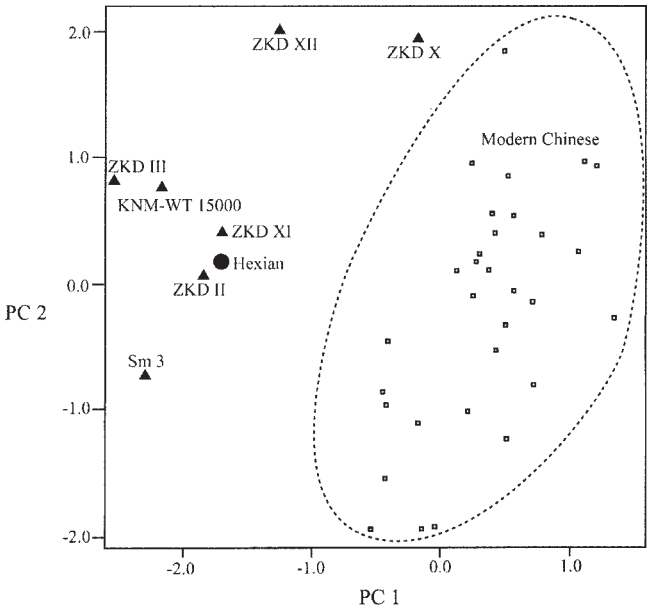

Fig. 12. Nine-variable PCA of Hexian, other *Homo erectus*, and modern Chinese. PC, principal component.

ent selective pressures that acted on the brain and the braincase during hominid evolution. Bookstein et al. (1999), in a study of the median-sagittal plane of the frontal bone in Neanderthals and modern humans, suggested that the forms of the inner and outer aspects of the bone are determined by entirely independent factors. More importantly, they argued that while external morphology is highly variable across taxa, the internal morphology of the frontal region (and thus inferably the anterior brain morphology) has been remarkably conservative over the past 500 ka, i.e., the period they viewed as the time when modern human cognitive capabilities evolved. Although our research methodology is not directly comparable to Bookstein et al. (1999), as we look at features of the entire anterior brain and compare specimens from different geographical regions, we document that the morphology of the frontal lobes displays some changes when later Asian *Homo erectus* is compared to modern humans. Specifically, for the Hexian and ZKD specimens, the surface of the frontal lobe is flatter, and there are prominent frontal and sagittal keels in addition to lower frontal heights and shorter frontal chords. Our results do not lend support to the

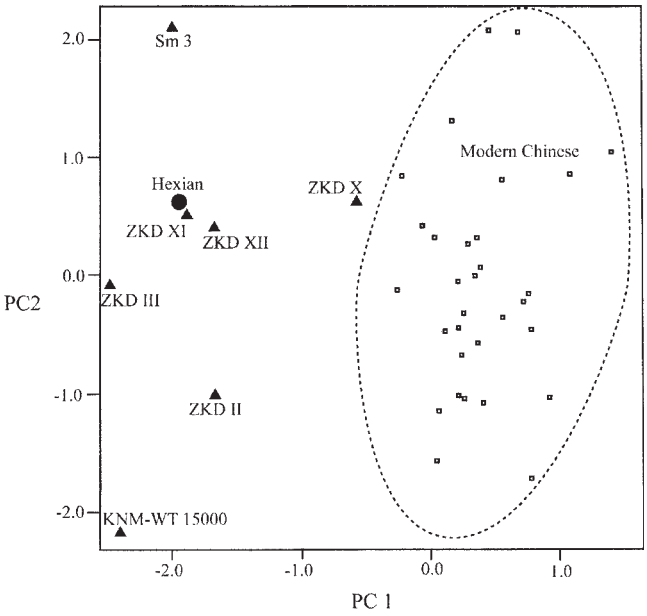

Fig. 13. Five-variable PCA of Hexian, other *Homo erectus*, and modern Chinese. PC, principal component.

conclusion of Bookstein et al. (1999) about the stability of anterior brain morphology. The occipital lobes were hypothesized to show a steady reduction during human evolution (Holloway, 1995), changing from a more posterior location (behind the parietal areas) to a more anterior position (under the parietal structures) in modern humans. The earlier morphology is seen in Hexian and the ZKD specimens, which all display strong posterior projections of the occipital lobes. Morphologically, Hexian is very similar to the ZKD endocasts in our analysis. This is consistent with the morphology of the calvarium itself, for which Hexian is more similar to ZKD than to the *Homo erectus* from Java (Wu and Dong, 1982; Wu and Poirier, 1995).

The metric data and nonparametric tests indicate that five variables (height, frontal breadth, cerebral height, frontal height, and parietal chord) and two indices (height-length index and breadth-height index) show statistical significance between *Homo erectus* and the modern Chinese in our sample. Form bivariate plot of height-length and height-breadth, the measurements most strongly differentiate modern Chinese males from *Homo erectus* specimens, and Hexian is metrically distinct from other *Homo erectus* relatively its breadth. This is consistent with other recent PCAs involving craniometrical data for Hexian and other *Homo erectus* specimens, where Hexian is again metrically distinct from other skulls relative to cranial breadth (Liu et al., 2005; Liu and Zhang, 2005). In the nine-variable PCA, that clustering mostly emphasizes height, frontal height, and frontal chord, Hexian clusters with Sm 3, ZKD III, ZKD XI, ZKD II, and KNM-WT 15000 relative to height, frontal height, and frontal chord. The five-variable PCA gives a clearer picture of the relationship of the specimens, where Hexian clusters with ZKD. Because all variables in the five-variable PCA are statistically significant, we may have more confidence that Hexian is metrically closest to the ZKD *Homo erectus* specimens, compared with the modern Chinese and other *Homo erectus*.

CONCLUSIONS

The geological age of Hexian is estimated at 412 ka, which is similar to Zhoukoudian (Grün et al., 1997; Huang et al., 1993), placing Hexian in the temporal range of Chinese *Homo erectus*. The endocast of Hexian possesses an endocranial volume of approximately 1,025 ml, which is in the middle of the range of endocranial volumes obtained for other *Homo erectus* specimens (Rightmire, 2004), and smaller than modern Chinese (Table 1). The Hexian endocast preserves many morphological features of taxonomic value. The key differences between Hexian and the modern Chinese include the following features of Hexian: 1) a low position of the greatest breadth and a low maximum height, 2) prominent frontal and sagittal keels, 3) flat frontal lobes, 4) depressed Sylvian areas and depressed surfaces of the parietal lobes, 5) strong posterior projection of the occipital lobes, 6) anterior positioning of the cerebellar lobes relative to the occipital lobes, and 7) relative simplicity of the meningeal vessels. Hexian shares many of these features with the ZKD specimens, and yet manifests some notable differences: the wide ovoid shape of Hexian that contrasts with the relatively long and narrow form of the ZKD endocasts; the flat Sylvian areas on Hexian that are distinct depressions on ZKD specimens; and differences in the forms of the occipital and temporal lobes. When the Hexian morphology is compared with KNM-WT 15000 and Sm 3, there are more differences involving overall shape, the relative flatness of the frontal lobes, the lack of frontal and sagittal keels that characterize Hexian, and the petalial and venous sinus patterns. The breadth-length index of Hexian is greater, and the height-breadth index is much lower, than in any of the other specimens. The metric distinctiveness of Hexian with respect to the other *Homo erectus* specimens is illustrated in the bivariate plot of height vs. breadth, and the five-variable PCAs. In conclusion, the morphological features of the Hexian endocast differ from those of modern Chinese and are comparable in many ways with other *Homo erectus* endocasts. Compared with ZKD, Indonesian, and African *Homo erectus* specimens, Hexian has more morphological features in common with the majority of ZKD specimens, as might be expected, given its temporal and geographical position. Metrically, *Homo erectus* are separated from the modern Chinese considerably with respect to the low height of *Homo erectus*. Hexian is close to ZKD and distinguished from other *Homo erectus* by its great breadth. Thus a combination of metrical and morphological data is needed to fully illustrate the variation in *Homo erectus* endocasts. Overall, the Hexian endocast resembles ZKD, both in morphology and in the metric pattern.

ACKNOWLEDGMENTS

We thank Yinyun Zhang and Zhongyi Zhao of the Institute of Vertebrate Paleontology and Paleoanthropology, Chinese Academy of Sciences, Beijing, who helped us reconstruct the endocasts. We also thank the staffs of the Department of Anthropology, University of Cincinnati, and the Department of Anthropology, Florida State University, for help and hospitality. We are grateful to Jinling Huang for her technical assistance.

LITERATURE CITED

Aboitiz F, Garcia GL. 1997. The evolutionary origin of language areas in the human brain. A neuroanatomical perspective. Brain Res Rev 25:381–396.

Adachi B. 1928. Das Arteriensystem der Japaner. Band 1. Kyoto: Verlag der Kaiserlich-Japanischen Universität zu Kyoto.

Amunts K, Schleicher A, Bürgel U, Mohlberg H, Uylings HBM, Zilles K. 1999. Broca's region revisited: cytoarchitecture and intersubject variability. J Comp Neurol 412:319–341.

Antón SC. 2002a. Evolutionary significance of cranial variation in Asian *Homo erectus*. Am J Phys Anthropol 118:301–324.

Antón SC. 2002b. Sambungmacan 3 and cranial variation in Asian *Homo erectus*. J Hum Evol 43:555–562.

Antón SC. 2003. Natural history of *Homo erectus*. Yrbk Phys Anthropol 46:126–170.

Begun D, Walker A. 1993. The endocast. In: Walker A, Leakey R, editors. The Nariokotome *Homo erectus* skeleton. Cambridge, MA: Harvard University Press. p 326–358.

Black D. 1930. Notice of the recovery of a second adult *Sinanthropus* skull specimen. Bull Geol Soc China 8:173–202.

Black D. 1931. On an adolescent skull of *Sinanthropus pekinensis* in comparison with an adult skull of the same species and with other hominid skulls, recent and fossil. Paleontol Sin Ser 7:1–144.

Black D. 1932. The brain cast of *Sinanthropus*. A review. J Comp Neurol 56:361–366.

Black D. 1933. On the endocranial cast of the adolescent *Sinanthropus* skull. Proc R Soc Lond [Biol] 112:263–276.

Bookstein F, Schäfer K, Prossinger H, Seidler H, Fieder M, Stringer C, Weber GW, Arsuaga JL, Slice D, Rohlf FJ, Recheis W, Mariam A, Marcus LF. 1999. Comparing frontal cranial profiles in archaic and modern *Homo* by morphometric analysis. Anat Rec (New Anat) 257:217–224.

Broadfield DC, Holloway RL, Mowbray K, Mowbray K, Silvers A, Yuan MS, Márquez S. 2001. Endocast of Sambungmacan 3 (Sm 3): a new *Homo erectus* from Indonesia. Anat Rec 262: 369–379.

Chen TM, Yuan SX, Gao SJ, Hu QY. 1987. Uranium-series data-lists on Hexian and Chaoxian, Anhui palaeolithic- and palaeo-anthropological sites. Acta Anthropol Sin 6:249–254.

Delson E, Harvati K, Reddy D, Marcus LF, Mowbray K, Sawyer GJ, Jacob T, Máquez S. 2001. The Sambungmacan 3 *Homo erectus* calvaria: a comparative morphometric and morphological analysis. Anat Rec 262:380–397.

Falk D. 1993. Meningeal arterial patterns in great apes: implications for hominid vascular evolution. Am J Phys Anthropol 92:81–97.

Falk D. 2006. Evolution of the primate brain. In: Henke W, Rothe H, Tattersall I, editors. Handbook of palaeoanthropology volume 2: primate evolution and human origin. Berlin: Springer-Verlag, in preparation.

Galaburda AM, LeMay M, Kemper TL, Geschwind N. 1978. Right-left asymmetries in the brain. Science 199:852–856.

Grün R, Huang PH, Wu XZ, Stringer CB, Thorne AG, McCulloch M. 1997. ESR analysis of teeth from the palaeoanthropological site of Zhoukoudian, China. J Hum Evol 32:83–91.

Grün R, Huang PH, Huang WP, McDermott F, Thorne A, Stringer CB, Yan G. 1998. ESR and U-series analyses of teeth from the palaeoanthropological site of Hexian, Anhui province, China. J Hum Evol 34:555–564.

Holloway RL. 1995. Toward a synthetic theory of human brain evolution. In: Chaneaux JP, Chavaillon J, editors. Origins of the human brain. Oxford: Clarendon Press. p 42–54.

Holloway RL, De La Coste-Lareyondie MC. 1982. Brain endocast asymmetry in pongids and hominids: some preliminary findings on the paleontology of cerebral dominance. Am J Phys Anthropol 58:101–110.

Huang PH, Jin SZ, Peng ZC, Liang RY, Lu ZJ, Wang ZR, Chen JB, Yuan ZX. 1993. ESR dating of tooth enamel: comparison with U-Series, FT and TL dating at the Peking Man site. Appl Radiat Isotopes 44:239–242.

Huang PH, Liang RZ, Zheng LZ, Quan YC, Xu YH, Fang YS, Fang NS. 1995. Study on age of Hexian *Homo erectus*. Acta Anthropol Sin 14:262–265.

Huang WP, Fang NS, Ye YX. 1981. Observations on the *Homo erectus* skull that was found from Longtandong, Hexian, Anhui. Chin Sci Bull 26:1508–1510.

Huang WP, Fang DS, Ye YX. 1982. Preliminary study on the fossil hominid skull and fauna of Hexian, Anhui. Vert Paleontol Asia 20:248–256.

Kidder JH, Durband AC. 2004. A re-evaluation of the metric diversity within *Homo erectus*. J Hum Evol 46:297–313.

LeMay M. 1976. Mophological cerebral asymmetries of modern man, and nonhuman primates. Ann NY Acad Sci 280:349–366.

LeMay M, Billing MS, Geschwind N. 1982. Asymmetries of the brains and skulls. In: Armstrong E, Falk D, editors. Primate brain evoluton. New York: Plenum Press. p 263–277.

Li HY, Mei Y. 1983. The upper age of Hexian *Homo erectus*. Chin Sci Bull 28:703.

Li Y, Chen S, Zhang K, Sun HB, Ni ZT, Chang WX. 2000. A study on morphological types of venous sinuses of the dural mater. J Shanghai Tiedao Univ 21:21–23.

Liu W, Zhang YY. 2005. The cranial metric diversity of Chinese *Homo erectus*. Acta Anthropol Sin 24:121–136.

Liu W, Zhang YY, Wu XZ. 2005. A middle Pleistocene human cranium from Tangshan, Nanjing, of southeast China: a comparisons with *Homo erectus* from Eurasia and Africa based on new reconstruction. Am J Phys Anthropol 127:253–262.

Rightmire GP. 2004. Brain size and encephalization in early to mid-Pleistocene *Homo*. Am J Phys Anthropol 124:109–123.

Weidenreich F. 1938. The ramification of the middle meningeal artery in fossil hominids and its bearing upon phylogenetic problems. Paleontol Sin New Ser D 3:1–16.

Weidenreich F. 1939. The phylogenetic development of the hominid brain and its connection with the transformation of the skull. Bull Geol Soc China 19:28–46.

Weidenreich F. 1943. The skull of *Sinanthropus pekinensis*: a comparative study on a primitive hominid skull. Paleontol Sin New Ser 10:108–113.

Wu RK, Dong XR. 1982. Preliminary study of *Homo erectus* remains from Hexian, Anhui. Acta Anthropol Sin 1:2–13.

Wu XZ, Poirier FE. 1995. Human evolution in China. New York: Oxford University Press. p 82–84.

Zilles K, Dabringhaus A, Geyer S, Amunts K, Qü M, Schleicher A, Gilissen E, Schlaug G, Steinmetz H. 1996. Structural asymmetries in the human forebrain and the forebrain of non-human primates and rats. Neurosci Biobehav Rev 20: 593–605.